Proceedings of ASME-JSME-KSME Joint Fluids Engineering Conference
ASME 2019/AJKFluids
July 28-August 1, 2019, San Francisco, USA

AJKFLUIDS2019-5615

DIRECTIONAL SURFACE ROUGHNESS INFLUENCE ON TURBULENT FLOW STRUCTURE

Zambri Harun*
Faculty of Engineering
and Built Environment
National University of Malaysia
UKM, Bangi, 43600, Malaysia
Email: zambri@ukm.edu.my

Ashraf A. Abbas
Faculty of Engineering
and Built Environment
National University of Malaysia
UKM, Bangi, 43600, Malaysia

Bagus Nugroho
Department of Mechanical Engineering
University of Melbourne
Victoria, 3010, Australia

ABSTRACT

A series of experiments have been conducted to investigate turbulent flow structures when it is exposed to a highly directional riblet-type surfaces roughness (converging-diverging/herringbone pattern) at a relatively low Reynolds number (Re_τ). These experiments show that even at a low Re_τ, the surface pattern is able to modify the turbulent boundary layer. Over the diverging region, we observe a decrease in drag penalty, while over the converging region there is an increase of drag penalty, which is indicated by the shift in the mean velocity profiles. The surface roughness also influences the turbulence production, indicated by the elevated turbulence intensities profiles for both the converging and diverging regions. The result seems to deviate from early investigations that show an increase in turbulence intensities above the converging region and a lowered turbulence intensities above the diverging region. The discrepancy may be caused by the lower Re_τ in the current report. Other important statistics such as skewness and flatness are also reported.

NOMENCLATURE

Re_τ Friction Reynolds number
δ Boundary layer thickness
U_τ Skin-friction velocity
τ_w Frictional wall shear stress
ρ Air density
α Riblet yaw angle
ν Kinematic viscosity
Λ Spanwise wavelength
s Riblet spacing
s^+ Viscous-scaled riblet spacing
h Riblet height
h^+ Viscous-scaled riblet height
l Hot-wire etched length
l^+ Hot-wire etched viscous-scaled length
d Hot-wire etched diameter
F_x Fetch distance
e Roughness offset

INTRODUCTION

This research is inspired by the concern over global warming phenomenon and atmospheric pollution which is related to the fuel burning, emission, and rising fuel cost, particularly in the last few decades. This situation has become central issues for the transport policy makers worldwide, for instance automotive [1], maritime [2–4] and aerospace [5–8]. As a result, it has sparked much research that are focused on a more green transportation system and environmentally friendly. For example, in the third phase of the emission trading session, the European Commission Emission Trading System (ETS) has set an ambitious 21% reduction in carbon pollutions by 2020. Furthermore, the Advisory Council for Aeronautics Research in Europe (ACARE), shows that this decade is the appropriate time to investigate new

*Address all correspondence to this author.

flow control technology that can achieve emissions reduction by 50% and 80% for CO_2 and NO_x by 2050 [9].

The fuel consumption is highly correlated to the relation of the skin friction drag between the flow and body, which is due to the interaction of the turbulent boundary layer over the body surface. The main challenge here is to overcome this resistance and to reduce the skin friction drag, where the viscous drag causes almost 50% of the total drag [8], in a streamlined body e.g. aircraft, ships and supertankers [10]. The integration of researches on the turbulent boundary layer interaction and the development of flow control technology could potentially reduce more than 40% of the viscous drag, which is equivalent to about 15% of the total drag. Hence, significant implications for fuel consumption are possible. A small ratio of this reduction could even be translated to saving of billions of dollars and promotes active recovery of the environments and sea life.

Turbulent flow control, particularly those that implement passive surface roughness, has been investigated intensively in the last five decades. One particular technique is by applying riblets surface, which is a surface roughness in the form of a corrugated wall and aligned in the direction of fluid flow. They are known to reduce skin friction drag by 7%-10% by modifying the near-wall small-scale structure of a turbulent boundary layer [11–14]. However, the potential of the conventional riblets surface to reduce the skin friction drag is still limited, particularly at high Reynolds number. Beyond certain Reynolds number thresholds, their drag reduction capability decreases and the riblets will behave like a regular (k-type) roughness. Hence regular riblets may not be suitable for a large engineering system such as aircraft. Moreover, recent progress in high Reynolds number studies shows that as Reynolds number increases, the near-wall small-scale structures are increasingly eclipsed by large-scale features [15].

Around a decade ago, a new class of riblet-type surface roughness was reported by Koeltzsch et al. [16], where they applied a herringbone patterned riblets inside the surface of turbulent pipe flow. This unique riblets feature is inspired from the skin pattern of a fast swimming shark that is located near their sensory part (i.e nose). The result shows that this pattern is able to force the fluid flow to move in an azimuthal direction and causing variation in the mean velocity, broadband turbulence intensities, and boundary layer thickness. Following this report, Nugroho et al. [17] extended their work and investigate the effect of the converging-diverging riblets subjected to zero pressure gradient (ZPG). They found that over the converging direction, the near-wall low-momentum flow is being pushed away from the wall, while over the diverging region the high-speed flow is being forced to move towards the surface. Overall, the results show that the herringbone pattern generates large-scale counter-rotating vortices that can influence the large-scale structure of turbulent flow. Following these reports, Kevin et al. [18] performed experiments using a stereoscopic particle image velocimetry (PIV) in the cross-stream plane at $Re_\tau \approx 3900$ over the converging-diverging riblets surface. They show that the directional riblets cause a modification over the entire boundary layer and rearranged turbulent structures. More over, the counter rotating vortices are found to be exist at only 25% over a certain period. Kevin [19] and co-workers extended their earlier investigations and found that the riblet surface caused instability of the boundary layer structure by meandering, breaking and branching the coherent structures. Beyond this, there have been several studies showing that the herringbone pattern is able to reduce skin friction drag by up to 16% [20,21]. Recent result performed by our turbulence team, Abbas et al. [22] on the NACA 0026 airfoil showed a high ability of riblets to modify the turbulence structure in the boundary layer. A breakdown of large-scale turbulence structures 20δ into smaller scales 3-4δ is feasible. This manipulation of flow structure needs to be understood further so that the ultimate aim to reduce the energy around the wing therefore increasing fuel efficiency can be achieved. Considering the potential effect of directional riblet-type surface roughness in various engineering applications, for instance, as a novel method of generating counter rotating roll-modes (vortices) for flow control purposes in aircraft wing, ship, tanker and turbine blade, it is crucial to investigate this pattern further.

In this study we are interested to extend the finding of Nugroho et al. [17]. Nugroho et al. [17] has performed experiments for Re_τ = 700 - 3000. In contrast, this paper restrict the variations so that Reynolds number effects are removed from the analysis.

EXPERIMENTAL SETUP

Flow Facility

The experiments were performed using the Pangkor low-speed wind tunnel (PLSWT) located at the Coastal and Water Resources laboratory of Faculty of Engineering and Built Environment, Universiti Kebangsaan Malaysia (UKM). Recently, we have developed our wind tunnel by adding a honeycomb device and four meshing screen to be in the overall of six screens built in the house, followed by a two-dimensional contraction nozzle with area ratio 2.4:1, which lead into a test section with cross-sectional area 1.2 m $\times$ 0.476 m (width $\times$ height) and 3m total length. The wind tunnel is fully automated with two-dimensional traverse system that is located at 1.7 m downstream to the inlet of the test section [23]. At free stream velocity U_∞ of 16 m/s, its free stream turbulence intensities are approximately 0.0085% different to the previous turbulence intensities value 5% [23]. The new value is suitable for the fundamental studies on the turbulent boundary layer. This wind tunnel was previously used by [22,24] and for further details, see [23]. Figure (1) shows the general arrangements of the wind tunnel.

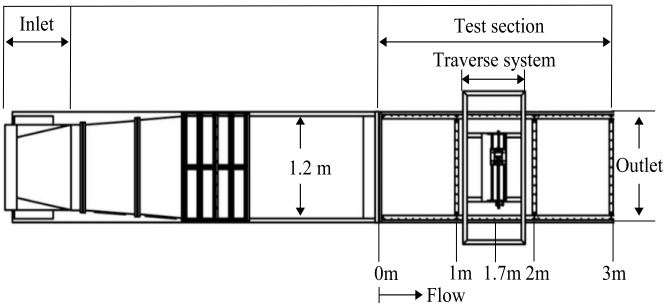

FIGURE 1. Schematic diagram of PLSWT geometry (side view).

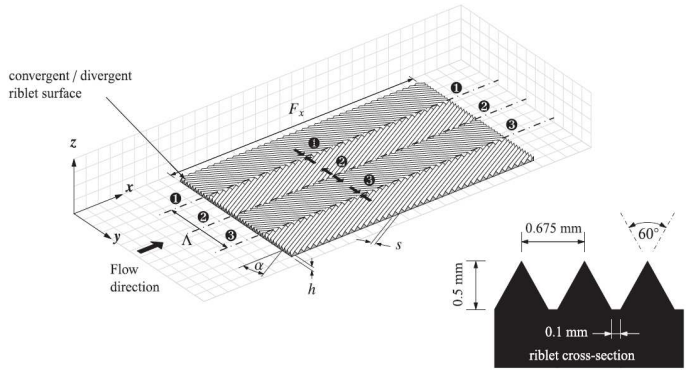

FIGURE 2. Schematic diagram of the converging–diverging riblet surface, showing expected regions of converging (regions ① & ③) and diverging (region ②). Inset shows the riblet cross-section. (Adapted from Nugroho et al. [17])

Roughness Surface Fabrication and Installation

In this experiment, we have used the same converging-diverging riblets surface previously used and studied by Nugroho et al. [17]. A three - axis high-precision $CNC-TechnikHEIZS-1000$ machine with a 60^o tool bit was used to create a master tile of the converging-diverging riblet pattern. The master tile has dimensions 515 $\times$ 295 mm containing two strips at $+\alpha$ and two strips at $-\alpha$ (the master tile dimension assures perfect tessellation in x and y). A mold of this tile was produced in platinum cured silicone rubber and used to cast multiple polyurethane reproductions of the original tile. The polyurethane is mixed with fine aluminium powder to assure more favourable mechanical properties. The resulting reproductions are then affixed to the floor of the boundary layer wind tunnel. The schematic in Figure. (2) shows the key dimensions for the surface. The cross-section of the riblets is trapezoidal, with a h/s ratio of 0.74. The riblet spacing s = 0.675 mm and height h = 0.5 mm. The other parameter is F_x, defined as the streamwise fetch. A detailed view of the riblet cross-section is also given in the inset of Figure. (2). The riblets (converging-diverging) are yawed at an angle $\alpha = \pm 10^o$, the width of each converging and diverging region is 74.75 mm (such that the repeating spanwise wavelength Λ = 149.5 mm).

The test surface comprises a total of 6 tiles with a distance of F_x = 1.5m. The riblet surface covers 67% spanwise width of the wind-tunnel test section with two tiles, or six complete spanwise wavelengths (6K), which covers $x/l = 50\%$ from the total length of the test section, where x = 1.5m is the total length of the riblets tiles and l = 3m is the total length of the test section. Plywood was used to eliminate the steps of the thickness of the tile.

EXPERIMENTAL PARAMETERS

Table 1 shows the experiment parameters for both the smooth-wall and herringbone surface type - riblets. The abbreviations S is for the smooth surface. C is for converging and D is for diverging, both yawed at angle $\alpha = \pm 10^o$. F_x is the streamwise fetch and U_∞ is free-stream velocity, h^+ is viscous-scaled riblet height, and s^+ is viscous-scaled riblet spacing, where $h^+ = hU_\tau/\nu$ and $s^+ = sU_\tau/\nu$. The boundary layer thickness is defined as δ where, calculated (based on the wall-normal location where the velocity recovers 99% of freestream velocity U_∞). The skin friction velocity is $U_\tau = \sqrt{\tau_w/\rho}$, (where τ_w is the wall shear stress and ρ is fluid density). The kinematic viscosity is ν, friction Karman number is Re_τ. For the existing experiments, wind tunnel operates at a free stream velocity of U_∞ = 5 m/s. Measurements were carried out with a locally fabricated sensor soldered onto a single hot-wire (Dantec's 55P05) boundary layer type probe. Using a Dantec's multi-channel constant temperature anemometer (CTA) system model 54N80, the overheat ratio is set within 1 - 1.5, similar to typical boundary layer studies [23, 25]. A wollaston wire (produced by Sigmund Cohn Corp) with a platinum core diameter of 5 microns (μm) were soldered to the tips of the hot-wire prong and then etched [26]. The hot-wire data is collected using National Instruments (NI) 9215 module while data from all other sensors such as temperature, static pressure (pitot-tube), atmospheric pressure, room humidity and dew point were collected using Comet, model H7331 [23]. This system allows measurement performed at very high frequency 20 kHz. It is important that high frequency is employed so that turbulence characteristics could be analyzed properly [27]. The hot-wire calibration was performed in-situ.

The hot-wire sensor was attached onto a two-dimensional traverse system, allowing it to move in both spanwise and wall normal direction. A Pitot tube, was attached at the center of the test section of the wind tunnel, allowing it to measure U_∞. Two calibrations were performed in-situ using the Pitot tube (pre-calibrations and post-calibrations), allowing us to overcome the error due to lengthy measurements caused by the change of atmospheric condition. The pre-calibrations (precal) were carried out prior to the boundary layer measurements. Temperatures, along with the atmospheric pressure and room humidity were also recorded during the precals. Another calibration process at

TABLE 1. Parameters for Smooth & Riblets Surface, $l^+ = lU_\tau/\nu \approx$ 12 – 14 and F_x = 1.5m for all.

Exp Code	Surface Type	U_∞ m/s	Re_τ	δ m	U_τ m/s	$\triangle U/U_\tau$
S □	Smooth	5.214	1218	0.087	0.224	
C ▷	Converging	5.015	1740	0.123	0.231	+ 0.603
D ○	Diverging	5.159	1192	0.099	0.195	- 1.729

the end of the experiment, the post-calibration (postcal), was also performed. The calibration curves were compared and, if necessary, temperature compensations might have to be implemented. Note that the calibration points are 10 points with the velocity incrementally from zero to slightly above freestream velocity ($\approx$ 200 % of U_∞). In each boundary layer measurement, the hot-wire sensor traverses 50 logarithmically spaced wall-normal positions starting at approximately 0.25 mm up to 200 mm. All measurements performed at a frequency of 20 kHz for 180 seconds. The hot wire positioning to the wall location have been followed the techniques suggested by [28]. To address spatial resolution issues appropriately, sensor lengths were etched to approximately l = 1 - 1.5 mm. Previous studies [29, 30] reported that the length-to-diameter ratio (l/d) of hot-wire sensor should exceed 200 to minimize attenuations due to end conduction effect. The sensor length has been controlled so as to follow the spatial resolution issues which are exacerbated in the APG environment [26]. The exposed sensor part for all measurements is l = 1 mm, results in non-dimensionalised sensor length $l^+ = lU_\tau/\nu \approx$ 12 - 14 for all flows.

RESULTS

Velocities and Intensities Profiles

Figure (3) shows the boundary layer mean velocity profiles over the smooth surface, converging region and diverging region of the riblets pattern. The vertical axis represents velocity; the overbar indicates mean value, therefore, $\overline{U}$ represents local mean velocity. The vertical axis of the boundary layer is made non-dimensional with the friction velocity U_τ obtained from the Clauser chart method, the lower abscissae is the scaled wall normal distance.

$$U^+ = \frac{1}{\kappa}\ln\left(\frac{zU_\tau}{\nu}\right) + A \tag{1}$$

In this study, the smooth-wall skin-friction velocity is obtained using the Clauser technique [31, 32], (see equation1), while the estimation the skin friction Uτ over the riblets is using modified Clauser technique (see equation 1). According to the previous study by [32], the mean velocity profile over a roughness surface need to be correlatable in U/U_τ, zU_τ/ν and eU_τ/ν, where e is the roughness offset parameter. The effect of this offset e is to shift the intercept A as a function of eU_τ/ν. Previous studies by [12, 33] shows that the roughness offset e can be calculated based on the shape of the riblet surface, i.e. $0.25h$ for triangular and $0.37h$ for scalloped riblets. The roughness offset in this study is chosen to be $e = 0.25h$, due to the triangular shape of riblets used in this experiment. The mean velocity profile is fitted to the logarithmic law and within the range of $0.38 < \kappa < 0.41$ and $4.1 < A < 6.5$, where κ is the Kármán constant and A is the wall intercept, [34]. In this study we use κ = 0.39 and an intercept A = 4.2. The vertical shift of the logarithmic curve that is caused by the roughness can be defined as $(roughness function)$ $\triangle U/U_\tau$. The addition of e and $\triangle U/U_\tau$ in the log-law (equation 1) results in a modified log-law:

$$U^+ = \frac{1}{\kappa}\ln\left(\frac{(z+e)U_\tau}{\nu}\right) + A - \frac{\triangle U}{U_\tau} \tag{2}$$

The results show that the converging-diverging riblets pattern has significant effects on the boundary layer thickness δ as well as to the skin friction velocity U_τ and Hama Roughness function $\Delta U^+ = \triangle U/U_\tau$, as shown in Table 1. The converging region above the riblets causes the local mean velocity to decrease and increase of drag, indicated by the downward shift of the mean velocity profile. The diverging region however, causes the local mean velocity to increase and the upward shift of the mean velocity profile indicates a decrease in drag penalty. These results are consistent with the finding of Nugroho et al [17], which indicate that over the diverging region there is a rush of high speed - low turbulent flows moving towards the surface while over the converging region the highly energetic low velocity flows are being pushed upwards. Interestingly however, the ΔU^+ shifts are not as high as Nugroho et al [17]. This is probably due to the lower Reynolds number.

$$U^+ = \frac{1}{\kappa}\ln\left(\frac{(z+e)U_\tau}{\nu}\right) + A + 1.7286 \tag{3}$$

$$U^+ = \frac{1}{\kappa}\ln\left(\frac{(z+e)U_\tau}{\nu}\right) + A - 0.6030 \tag{4}$$

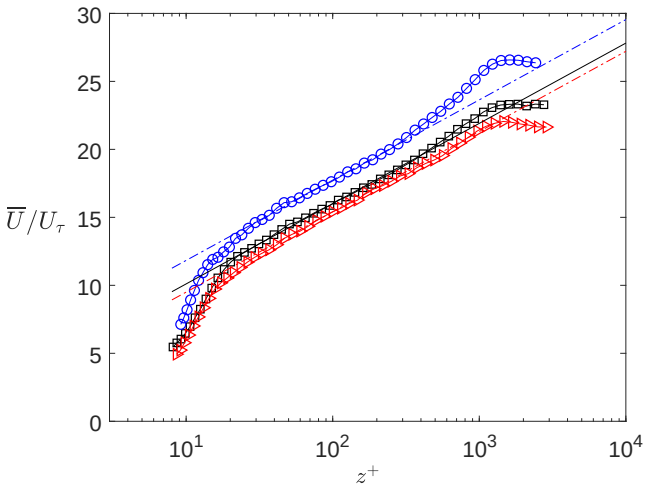

FIGURE 3. Mean velocity profile for (□) smooth, (▷) converging riblets and (○) for diverging riblets. The solid black line indicates the log law for the smooth surface, while The blue and red dashed dot line for the modified log law for diverging & converging riblets respectively, here $\kappa = 0.39$ and $A = 4.2$.

Figure (4) shows turbulence intensities profiles for flows past the smooth surface and the converging-diverging riblets. The vertical axis represents the broadband turbulence intensities profile, $\overline{u}^2/U_\tau^2$. The near-wall turbulence intensities for flow past a smooth surface, $\overline{u}^2/U_\tau^2|_{\text{max,S}} \approx 8.25$ at $z^+ = 15$. Which is within the acceptable range of the turbulence intensities $\overline{u}^2/U_\tau^2 \approx 7$ - 10 [25, 35–37]. The turbulence intensities profiles of the rough wall however, are found to behave differently compared to that of Nugroho et al [17] findings. Here the broadband turbulence intensities profile of the diverging region is higher than that of converging region and the smooth wall. Moreover, this happens over the entire boundary layer. It seems that at this particular Reynolds number, the diverging region is unable to force the high speed and low turbulence intensities flow moves towards the surface.

Skewness and Flatness

In this section, we are interested in looking at the higher order turbulence statistics of the flow over the riblet surface. The boundary layer velocity profile has shown that the converging-diverging patterns are significantly affect and modify the velocity profile compared with the smooth surface.

Addition to this the turbulence intensities indicate that the averages strength of the fluctuations but it cannot tell whether these fluctuations are alternating equally about the mean value, dominated by rare positive fluctuations (with frequent negative ones) or the reverse. In addition, the intensity does not elucidate if turbulence fluctuations are of random scales, dominated by intermittent large fluctuations (with long silence periods) or

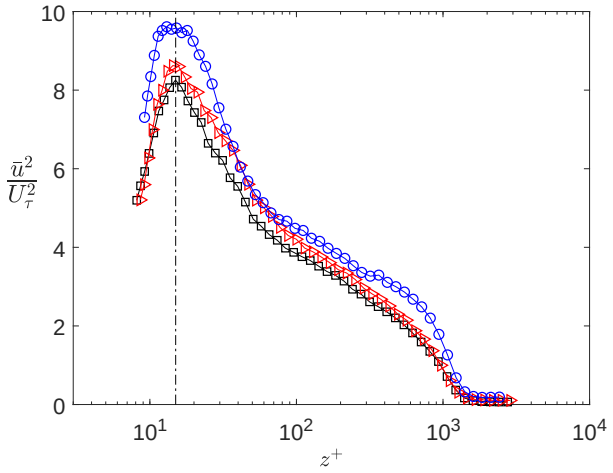

FIGURE 4. Broadband turbulence intensities profile over (□) smooth, (▷) converging riblets and (○) for diverging riblets. The dashed dot line at $z^+ = 15$

continuous small ones. Here comes, respectively, the importance of the *skewness* factor, S_u, and *flatness* factor, F_u defined as:

$$S_u = \frac{\overline{u^3}}{\left(\overline{u^2}\right)^{3/2}}, \qquad F_u = \frac{\overline{u^4}}{\left(\overline{u^2}\right)^2} \tag{5}$$

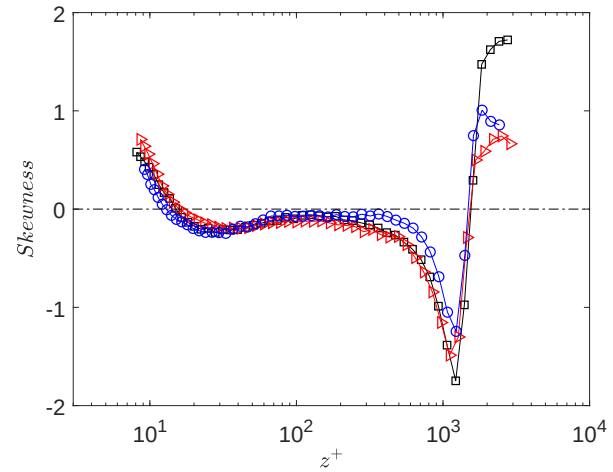

FIGURE 5. Skewness S_u profile, (□) smooth, (▷) converging riblets and (○) diverging riblets.

If the turbulence statistics, follow a Gaussian distribution, the skewness and flatness coefficients of u distribution, will

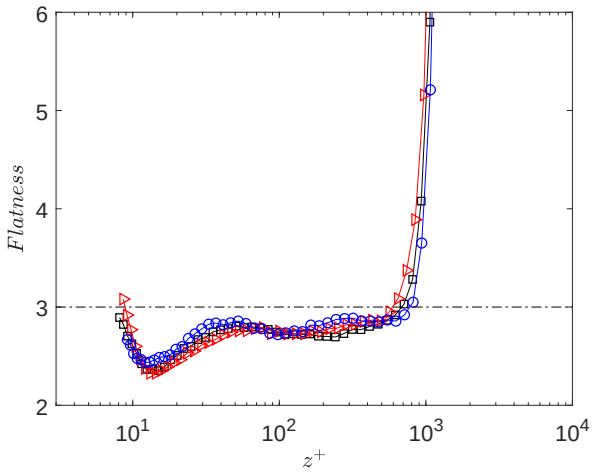

FIGURE 6. Flatness F_u (□) smooth, (▷) converging riblets and (○) for diverging riblets.

achieve values of $S_u = 0$, if $\overline{u^3} = 0$. However, flatness F_u will attain a greater value than the Gaussian value of 3 [38]. Figure (5) shows the skewness factors of the streamwise velocity fluctuation over the smooth surface and the herringbone riblets pattern(converging & diverging), where the positive skewness near-wall region and negative skewness at the boundary layer edge clearly appear, due to the influence of riblets surface (converging & diverging) in the nearwall and wake region. The riblets (converging & diverging) has a high contribution in modifying the boundary layer structure and increase the S_u in the log-regions, especially the converging riblets, causes to raise the skewness coefficients, however the diverging riblets work to reduce the and extend the skewness coefficients in the logarithmic region, where $S_u \approx 0$ in the log region and this could offer a Gaussian characteristic. For all cases, smooth surface and any of riblets type, show non-Gaussian distributions for both near wall and an outer region. It seems that for converging riblet, the near wall larger skewness coefficients here, although small but noticeable, agree with the findings by Nugroho [39]. This is also similar to the effects of Reynolds number and adverse pressure gradients where Monty et al. [25] attributed to the increased large-scale influence in the near-wall region.

The flatness F_u of the streamwise velocity fluctuation shown in figure (6) reveal a tendency towards large positive intermittent motions and large negative intermittent motions in these regions, respectively [40]. In the near wall region, the diverging riblets play the main role, where it causes the flatness coefficient to rise and to extend the logarithmic region. However, less effect could be seen by the converging riblets for the entire boundary layer. It is evident that the riblets cause to rearrange the flow structure. Resulting in a non-Gaussian distribution for all three cases. Again, the near wall effects here is similar to the Re_τ and pressure gradient effects [25].

Conclusion

A series of experiments to investigate the effect of a riblet-type surface roughness with herringbone/converging-diverging pattern, on favourable pressure gradient (FPG) turbulence boundary layer were conducted using hot-wire anemometer. The results indicate that the pattern causes large-scale counter rotating vortices in which the converging region form the common-flow-up and the diverging region form the common-flow-down. The mean velocity profiles show that the diverging region experiences a lower drag penalty while the converging region experiences a higher drag penalty, akin to the finding by Nugroho et al [17]. The main differences however, the low Re_τ in this study results in a relatively low ΔU_τ shift for both the diverging and converging region. Interestingly however, the turbulence intensities does not behave as we expected, above the diverging region, the turbulence intensities are higher than that of smooth wall and converging region. This result is the opposite from what is reported by Nugroho et al [17]. We believe that this is caused by the low Re_τ, the roughness is not strong enough to force and push the low turbulence intensities closer closer to the surface. The higher statistics however show similar statistics as compared with the existing literatures. The near-wall effect of a flow exposed to converging riblets have larger skewness and flatness coefficients, similar to Re_τ number and adverse pressure gradient effects.

The herringbone patterned riblet type surface roughness has the potential to be a novel method of generating counter-rotating roll-modes from an extremely low profile device. Such surfaces may eventually present an interesting addition to the different flow control techniques.

ACKNOWLEDGMENT

We would like to express our gratitude for the financial supports provided by the Ministry of Higher Education's fundamental research grant FRGS/1/2016/TK03/UKM/02/1, Ministry of Science Science, Technology, and Innovation (MOSTI) Science Fund grant 06-01-02-SF1326, and Research University Grant GUP-2018-102.

REFERENCES

[1] Michaelis, P., and Zerle, P., 2006. "FromACEA's voluntary agreement to an emission trading scheme for new passenger cars". *Journal of Environmental Planning and Management,* ***49***, pp. 435–453.

[2] Longva, T., Eide, M. S., and Skjong, R., 2010. "Determining a required energy efficiency design index level for new ships based on a cost-effectiveness criterion". *Maritime Policy & Management,* ***37***, pp. 129–143.

[3] Nugroho, B., Ganapathisubramani, B., Utama, I. K. A. P., Suastika, I. K., Yusuf, M., Tullberg, M., Monty, J. P., and Hutchins, N., 2017. "Managing international collaborative research between academics, industries, and policy makers in understanding the effects of biofouling in ship hull turbulent boundary layers". *International Journal of Maritime Engineering,* ***159***, pp. 291–300.

[4] Sun, Y., Yan, X., Yuan, C., and Bai, X., 2018. "Insight into tribological problems of green ship and corresponding research progresses". *Friction*, pp. 1–12.

[5] Preston, H., Lee, D. S., and Hooper, P. D., 2012. "The inclusion of the aviation sector within the European Union's Emissions Trading Scheme: What are the prospects for a more sustainable aviation industry?". *Environmental Development,* ***2***, pp. 48–56.

[6] Malina, R., McConnachie, D., Winchester, N., Wollersheim, C., Paltsev, S., and Waitz, I. A., 2012. "The impact of the European Union emissions trading scheme on US aviation". *Journal of Air Transport Management,* ***19***, pp. 36–41.

[7] Abbas, A., De Vicente, J., and Valero, E., 2013. "Aerodynamic technologies to improve aircraft performance". *Aerospace Science and Technology,* ***28***, pp. 100–132.

[8] Abbas, A., Bugeda, G., Ferrer, E., Fu, S., Periaux, J., Pons-Prats, J., Valero, E., and Zheng, Y., 2017. "Drag reduction via turbulent boundary layer flow control". *Science China Technological Sciences,* ***60***, pp. 1281–1290.

[9] Kallas, S., Geoghegan-Quinn, M., Darecki, M., Edelstenne, C., Enders, T., Fernandez, E., and Hartman, P., 2011. Flightpath 2050 Europe's Vision for Aviation, Report of the High Level Group on Aviation Research, European Commission, Brussels, Belgium, Report No. EUR 98.

[10] Harun, Z., Abbas, A. A., Nugroho, B., Chan, L., and Mat, S., 2018. "Surface roughness effects studies in transportation industries". *Jurnal Kejuruteraan,* ***1***(7).

[11] Walsh, M. J., 1983. "Riblets as a viscous drag reduction technique". *AIAA Journal,* ***21***(4), pp. 485–486.

[12] Choi, K.-S., 1989. "Near-wall structure of a turbulent boundary layer with riblets". *Journal of Fluid Mechanics,* ***208***, pp. 417–458.

[13] Bechert, D. W., Bruse, M., Hage, W. v., Van der Hoeven, J. G. T., and Hoppe, G., 1997. "Experiments on drag-reducing surfaces and their optimization with an adjustable geometry". *Journal of Fluid Mechanics,* ***338***, pp. 59–87.

[14] Bechert, D. W., Bruse, M., and Hage, W., 2000. "Experiments with three-dimensional riblets as an idealized model of shark skin". *Experiments in Fluids,* ***28***(5), pp. 403–412.

[15] Hutchins, N., Chauhan, K., Marusic, I., Monty, J., and Klewicki, J., 2012. "Towards reconciling the large-scale structure of turbulent boundary layers in the atmosphere and laboratory". *Boundary-Layer Meteorol,* ***145***(2), pp. 273–306.

[16] Koeltzsch, K., Dinkelacker, A., and Grundmann, R., 2002. "Flow over convergent and divergent wall riblets". *Experiments in Fluids,* ***33***(2), pp. 346–350.

[17] Nugroho, B., Hutchins, N., and Monty, J. P., 2013. "Large-scale spanwise periodicity in a turbulent boundary layer induced by highly ordered and directional surface roughness". *International Journal of Heat and Fluid Flow,* ***41***, pp. 90–102.

[18] Kevin, K., Monty, J. P., Bai, H. L., Pathikonda, G., Nugroho, B., Barros, J. M., Christensen, K. T., and Hutchins, N., 2017. "Cross-stream stereoscopic particle image velocimetry of a modified turbulent boundary layer over directional surface pattern". *Journal of Fluid Mechanics,* ***813***, pp. 412–435.

[19] Kevin, K., Monty, J., and Hutchins, N., 2019. "Turbulent structures in a statistically three-dimensional boundary layer". *Journal of Fluid Mechanics,* ***859***, pp. 543–565.

[20] Chen, H., Rao, F., Shang, X., Zhang, D., and Hagiwara, I., 2013. "Biomimetic drag reduction study on herringbone riblets of bird feather". *Journal of Bionic Engineering,* ***10***(3), pp. 341–349.

[21] Chen, H., Rao, F., Shang, X., Zhang, D., and Hagiwara, I., 2014. "Flow over bio-inspired 3D herringbone wall riblets". *Experiments in Fluids,* ***55***(3), p. 1698.

[22] Abbas, A. A., Ghopa, W. A. W., Mat, S., Choi, K.-S., Abdullah, M. F., and Harun Z., ., 2018. "Surface roughness effects on turbulent boundary layer structure of NACA 0026 Airfoil". *International Journal of Engineering & Technology(UAE),* ***7***(3.17), pp. 254–259.

[23] Harun, Z., W. Ghopa, W. A., Abdullah, A., Ghazali, M. I., Abbas, A. A., Rasani, M. R., Zulkifli, R., Wan Mahmood, W. M. F., Abu Mansor, M. R., Zainol Abidin, Z., and Wan Mohtar, W. H. M., 2016. "The development of a multipurpose wind tunnel". *Jurnal Teknologi,* ***10***, pp. 63–70.

[24] Harun, Z., Abbas, A. A., Dheyaa, R. M., and Ghazali, M. I., 2016. "Ordered roughness effects on NACA 0026 airfoil". In IOP Conference Series: Materials Science and Engineering, Vol. 152, IOP Publishing, p. 012005.

[25] Monty, J. P., Harun, Z., and Marusic, I., 2011. "A Parametric Study of Adverse Pressure Gradient Turbulent Boundary Layers". *International Journal of Heat and Fluid Flow,* ***32***(3), pp. 575–585.

[26] Harun, Z., Isa, M. D., Rasani, M. R., and Abdullah, S., 2012. "The effects of spatial resolution in turbulent boundary layers with pressure gradients". In Applied Mechanics and Materials, Vol. 225, Trans Tech Publ, pp. 109–117.

[27] Lin, W.-p., White, B., and Bagheri, N., 1995. "Experiments on the large-scale structure of turbulent boundary layers with adverse pressure gradients". In 33rd Aerospace Sciences Meeting and Exhibit, p. 21.

[28] Hutchins, N., and Choi, K.-S., 2002. "Accurate measurements of local skin friction coefficient using hot-wire

anemometry". *Progress in Aerospace Sciences*, ***38***(4-5), pp. 421–446.
[29] Ligrani, P. M., and Bradshaw, P., 1987. "Spatial resolution and measurement of turbulence in the viscous sublayer using subminiature hot-wire probes". *Experiments in Fluids*, ***5***(6), pp. 407–417.
[30] Hutchins, N., Nickels, T. B., Marusic, I., and Chong, M. S., 2009. "Hot-wire spatial resolution issues in wall-bounded turbulence". *Journal of Fluid Mechanics*, ***635***, pp. 103–136.
[31] Clauser, F. H., 1954. "Turbulent boundary layers in adverse pressure gradients". *Journal of the Aeronautical Sciences*, ***21***(2), pp. 91–108.
[32] Clauser, F. H., 1956. "The turbulent boundary layer". In *Advances in Applied Mechanics*, Vol. 4. Elsevier, pp. 1–51.
[33] Bechert, D., and Reif, W., 1985. "On the drag reduction of the shark skin". In 23rd Aerospace Sciences Meeting, p. 546.
[34] Nagib, H. M., and Chauhan, K. A., 2008. "Variations of von Kármán coefficient in canonical flows". *Physics of Fluids*, ***20***(10), p. 101518.
[35] Harun, Z., Monty, J. P., and Marusic, I., 2011. "The structure of zero, favorable and adverse pressure gradient turbulent boundary layers". In TSFP Digital Library Online, Begel House Inc.
[36] Harun, Z., Marusic, I., Monty, J. P., and Mathis, R., 2012. "Effects of pressure gradient on higher order statistics in turbulent boundary layers". In ICHMT Digital Library Online, Begel House Inc.
[37] Harun, Z., Monty, J. P., Mathis, R., and Marusic, I., 2013. "Pressure gradient effects on the large-scale structure of turbulent boundary layers". *Journal of Fluid Mechanics*, ***715***, pp. 477–498.
[38] Fernholz, H. H., and Finleyt, P. J., 1996. "The incompressible zero-pressure-gradient turbulent boundary layer: an assessment of the data". *Progress in Aerospace Sciences*, ***32***(4), pp. 245–311.
[39] Nugroho, B., 2015. "Highly ordered surface roughness effects on turbulent boundary layers". PhD thesis, University of Melbourne, Parkville.
[40] Klebanoff, P., 1955. Characteristics of turbulence in a boundary layer with zero pressure gradient. Tech. rep., National Bureau of Standards Gaithersburg MD.